Advances in Materials
2026, Vol. 15, No. 3, pp. 99–109
https://doi.org/10.11648/j.am.20261503.13

SciencePG
Science Publishing Group

Research Article

Growth Time-dependent Structural and Optical Properties of Hydrothermally Synthesized ZnO Thin Films

Mazabalo Baneto[1, 2, *], Jeanne Senam Aklamanu[1, 2], Alphonse Déssoudji Gboglo[1, 2], Ognanmi Ako[1, 2], Abdoul-Razak Ali-Tagba[1, 2], Monneka Fiacre Kouide[1, 2], Danoka Djagbai[1, 2], Makadatièna Badjemna[1, 2], Akotchayé Amenou[1, 2]

[1]Centre d'Excellence Régional Pour la Maîtrise de l'Electricité (CERME), University of Lomé, Lomé, Togo
[2]Laboratory on Solar Energy, Department of Physics, Faculty of Sciences, University of Lomé, Lomé, Togo

Abstract

The present study investigates the influence of growth time on the physical properties of ZnO thin films grown by the hydrothermal method. Film fabrication is carried out via a two-step process involving the deposition of ZnO seed layers on glass substrates by spin coating, followed by hydrothermal growth. Post-deposition annealing at 400°C for 3 hours is performed to enhance crystallinity. Structural and optical properties are analyzed using X-ray diffraction (XRD), UV–visible spectroscopy, and photoluminescence (PL) spectroscopy. XRD results confirm that all films are polycrystalline with a hexagonal wurtzite structure and exhibit a pronounced preferential orientation along the (002) plane. The progressive increase in the (002) peak intensity with growth time indicates enhanced crystalline quality, accompanied by an increase in crystallite size from 11.19 to 14.67 nm. UV–visible analysis shows that transmittance decreases from 95% to 65% with increasing growth time, mainly due to increased film thickness and density. However, films grown between 2 and 5 hours provide a good compromise between high transmittance in the visible region and strong absorption in the ultraviolet region. The optical bandgap varies from 3.14 eV to 3.27 eV, attributed to changes in film thickness. PL spectra exhibit three emission bands centered at 412 nm (3.01 eV), 438 nm (2.83 eV), and 490 nm (2.53 eV), associated with intrinsic defects in ZnO. The films grown for 4 hours exhibit relatively low defect density and good visible transmittance, making them promising candidates for photovoltaic applications.

Keywords

Thin Film, Zinc Oxide, Growth Time, Physical Properties, Hydrothermal, Photovoltaic Applications

1. Introduction

The rapid development of photovoltaic technologies over recent decades has intensified the search for alternative materials capable of improving device efficiency while reducing fabrication costs [1]. In this context, nanotechnology has emerged as a promising approach, particularly through the integration of semiconductor materials into photovoltaic devices [2]. Among semiconductor oxides, titanium dioxide (TiO_2) remains the most widely used material for photoanode

*Correspondence: Mazabalo Baneto (mazbaneto@gmail.com)

Received: 14 June 2026; **Accepted:** 25 June 2026; **Published:** 18 August 2026

fabrication in photovoltaic cells because of its good chemical stability and suitable electronic properties [3]. However, zinc oxide (ZnO), an n-type semiconductor, has attracted considerable attention as a potential alternative owing to its remarkable physical properties, including a wide direct bandgap (~3.37 eV), high exciton binding energy (~60 meV), high electron mobility (~205 $cm^2 \cdot V^{-1} \cdot s^{-1}$), and excellent thermal and mechanical stability [4, 5]. In addition to these intrinsic properties, ZnO thin films exhibit high optical transparency in the visible region and strong ultraviolet absorption, making them suitable for optoelectronic and photovoltaic applications. Furthermore, ZnO can be synthesized using various low-cost and scalable deposition techniques, allowing better control of its structural and optical characteristics. These advantages make ZnO a promising candidate for photoanode applications in photovoltaic devices [6].

The structural and optical properties of ZnO thin films strongly depend on the synthesis technique and deposition conditions. Several methods have been employed for the fabrication of ZnO films, including thermal evaporation [7], sputtering [8], pulsed laser ablation [9], chemical vapor deposition [10], sol-gel [11], spray pyrolysis [12], chemical bath deposition [13] and hydrothermal [14, 15]. Among these techniques, the hydrothermal method has emerged as a particularly attractive route because of its simplicity, low cost, low-temperature processing, and ability to produce highly crystalline ZnO films with preferential orientation. Despite these advantages, controlling the physical properties of hydrothermally synthesized ZnO films remains a significant challenge. Several parameters, such as precursor concentration, solution pH, growth temperature, and growth time, strongly influence the crystalline quality, optical transparency, defect density, and overall film performance [16]. In particular, the use of a ZnO seed layer has been reported to improve film adhesion, promote oriented growth, and enhance crystallinity [17].

Previous studies have demonstrated that growth time plays a crucial role in determining the properties of hydrothermally synthesized ZnO films. Dloo et al. [18] reported that increasing growth time significantly affects the dimensions and density of ZnO nanowires, leading to an increase in both their length and diameter. Similarly, Amin et al. [19] observed a nearly linear relationship between growth duration and the increase in the dimensions of ZnO structures for growth times up to 10 h. Linhua Xu et al. [15] further demonstrated that prolonged growth duration enhances the c-axis crystalline orientation and improves the crystalline quality of ZnO films. Abdel-Fattah and Alshehri [20] showed that extending the hydrothermal reaction time induces a progressive evolution of ZnO nanostructures from nanoparticles to nanoneedles, nanoflakes, and nanoplates, accompanied by significant changes in crystallographic orientation, which ultimately influence the photocatalytic performance. More recently, Zeid et al. [21] investigated the time-dependent growth of ZnO nanowires and established correlations between growth duration, nanowire morphology, photocatalytic activity, and antibacterial performance. Their results confirmed that growth time strongly influences the structural quality and defect concentration of hydrothermally synthesized ZnO nanostructures. Although several studies have investigated the influence of growth conditions on hydrothermally synthesized ZnO films, greater attention has primarily been devoted to their morphological evolution. In contrast, comparatively limited attention has been paid to identifying the optimal growth duration capable of simultaneously enhancing crystallinity, reducing defect density, and maintaining high visible transparency for photovoltaic applications.

Therefore, the present work aims to systematically investigate the effect of growth time on the structural and optical properties of ZnO thin films synthesized using a combined spin-coating and hydrothermal process. Unlike previous studies that mainly focused on morphological evolution and functional performance, this work establishes a comprehensive and quantitative correlation between growth time and the intrinsic structural and optical properties of ZnO thin films. In particular, correlations are systematically analyzed between growth duration, texture coefficient, crystallite size, dislocation density, and defect-related photoluminescence emissions, in order to identify the optimal growth conditions for enhanced crystalline quality and optical performance, which are essential requirements for photovoltaic photoanode applications.

2. Materials and Methods

2.1. Materials and Reagents

Microscope glass slides were used as substrates for ZnO thin film deposition. Zinc nitrate hexahydrate ($Zn(NO_3)_2 \cdot 6H_2O$, 99.99%) was used as the zinc precursor, while hexamethylenetetramine (HMTA, 99%) served as the complexing agent during hydrothermal growth. Zinc acetate dihydrate was employed for the preparation of the ZnO seed layers. Ethanol (98.8%), acetone (99.5%), and distilled water were used as solvents and cleaning agents. All chemicals were of analytical grade and purchased from Thermo and Fisher Scientifics without further purification.

2.2. Substrate Cleaning

Glass substrates were cut into dimensions of 4.5 cm × 2.5 cm using a diamond glass cutter to fit the autoclave configuration employed during hydrothermal synthesis. Prior to deposition, the substrates were ultrasonically cleaned for 15 min successively in soapy water, distilled water, acetone, ethanol, and distilled water to remove residual contaminants and ensure good surface cleanliness. The substrates were then dried under ambient conditions before deposition. This cleaning procedure is essential since the physical properties of ZnO thin films strongly depend on substrate surface quality.

2.3. ZnO Seed Layers Preparation

The ZnO seed layers were deposited onto the cleaned glass substrates using the spin-coating technique. Figure 1 schematically illustrates the preparation procedure. A 10 mM precursor solution was prepared by dissolving 0.044 g of zinc acetate dihydrate in 20 mL of ethanol. The solution was magnetically stirred at room temperature for 20 min until a clear and homogeneous solution was obtained. For deposition, a few drops of the precursor solution were dispensed onto the substrate surface, followed by spin coating at 1500 rpm for 45 s to ensure uniform film formation. After each coating cycle, the deposited layer was dried on a hot plate at 150°C for 2 min to evaporate residual solvents. This deposition/drying cycle was repeated 10 times to obtain homogeneous ZnO seed layers [22].

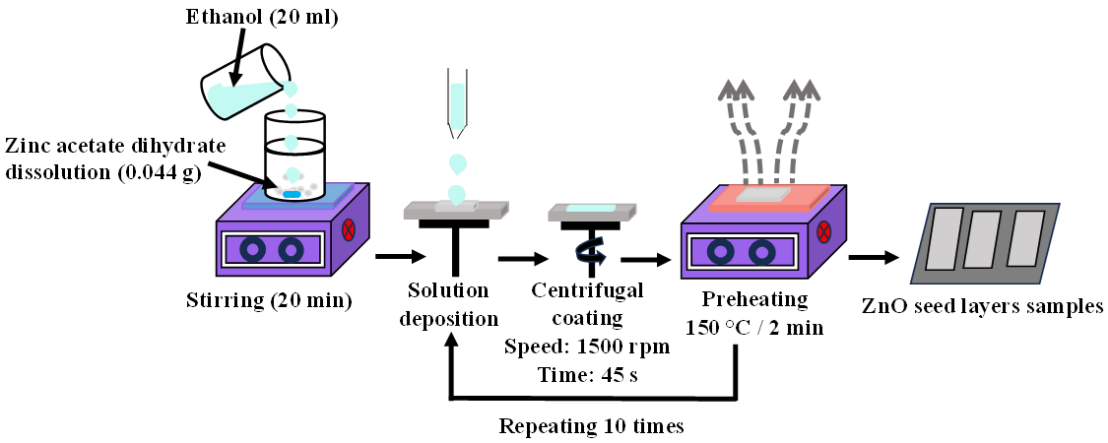

Figure 1. Schematic illustration of ZnO seed layers spin coated.

2.4. Growth of ZnO Thin Films

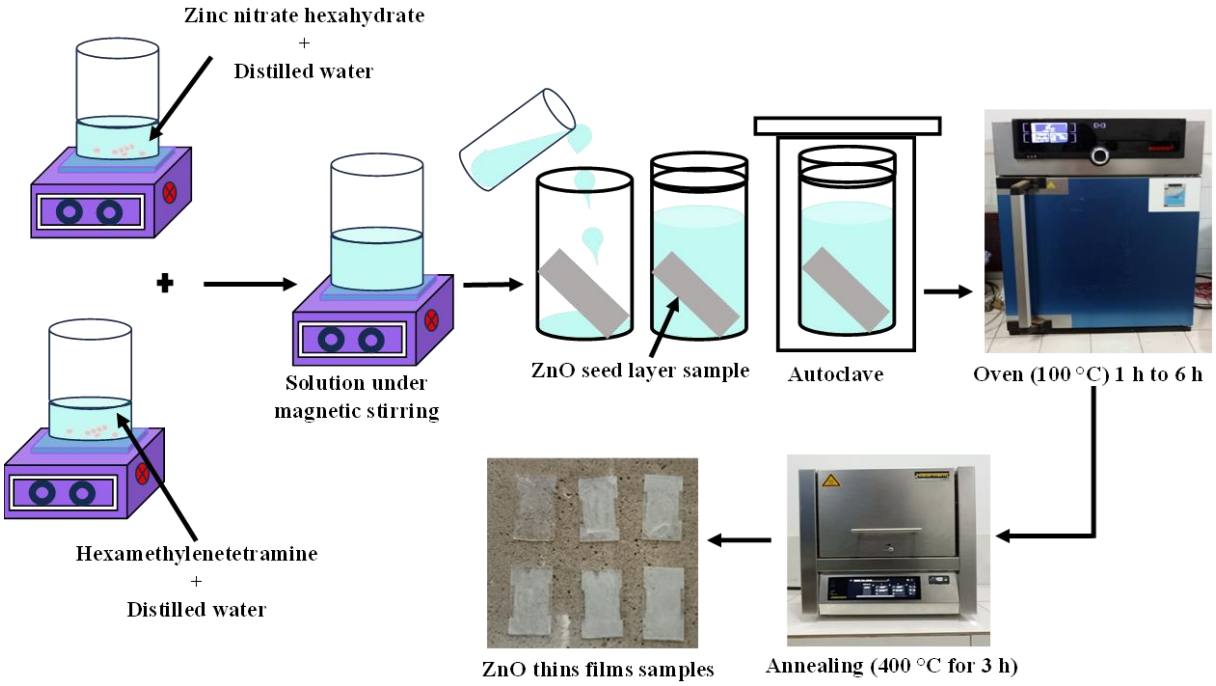

Figure 2. Schematic illustration of the hydrothermal growth process of ZnO thin films.

The hydrothermal method is a solution-based synthesis process involving the heating of aqueous precursor solutions in a sealed vessel (autoclave) under controlled temperature conditions. In the present study, ZnO thin films were synthesized

using precursor solutions with a concentration of 0.1 M, prepared from an equimolar mixture of zinc nitrate hexahydrate to HMTA. The zinc precursor solution was prepared by dissolving 2.975 g of $Zn(NO_3)_2 \cdot 6H_2O$ in 50 mL of distilled water under magnetic stirring. Separately, 1.402 g of HMTA was dissolved in 50 mL of distilled water under identical conditions. The two solutions were subsequently mixed and continuously stirred until a clear and homogeneous solution was obtained. Figure 2 schematically illustrates the hydrothermal growth process of the ZnO thin films. The prepared solution was transferred into a Teflon-lined vessel. Glass substrates previously coated with ZnO seed layers were then immersed vertically in the solution. The upper surface of each substrate was covered with adhesive tape in order to promote ZnO deposition exclusively on the lower surface. The Teflon vessel was sealed inside a stainless-steel autoclave and placed in an oven maintained at 100°C. Hydrothermal growth was carried out for durations ranging from 1 to 6 h. After the completion of the growth process, the autoclave was removed from the oven and allowed to cool naturally to room temperature before recovering the deposited films.

2.5. Characterization of ZnO Thin Films

The structural properties of the synthesized ZnO thin films were investigated using X-ray diffraction (XRD) analysis with a RIGAKU SmartLab diffractometer employing CuKα radiation with a wavelength of λ=1.54059 Å. The diffraction patterns were recorded over a 2θ range of 10°–90° at room temperature in order to identify the crystalline phases and evaluate the structural quality of the films. The optical properties of the ZnO thin films were analyzed at room temperature using a dual-beam UV–visible spectrophotometer (LAMBDA® 365+ model). The transmittance spectra were recorded in the wavelength range of 300–1100 nm to investigate the optical transparency and absorption behavior of the deposited films. Photoluminescence (PL) measurements were performed using an Ocean Optics spectrometer equipped with a 405 nm diode laser excitation source. PL spectroscopy was employed to evaluate the defect-related optical emissions and investigate the presence of intrinsic defects in the ZnO thin films.

The degree of preferential orientation of the crystallites along the (hkl) planes was evaluated using the texture coefficient $T_{C(hkl)}$, calculated from the diffraction peak intensities according to Equation (1) [23]:

$$T_{C(hkl)} = \frac{\left[\frac{I_{(hkl)}}{I_{r(hkl)}}\right]}{\frac{1}{n}\left[\Sigma_n\left(\frac{I_{(hkl)}}{I_{r(hkl)}}\right)\right]} \quad (1)$$

where $I_{(hkl)}$ represent the XRD intensities obtained from the thin films, n is the number of diffraction peaks considered, and $I_{r(hkl)}$ is the XRD reference intensity (JCPDS card No. 36-1451) for randomly oriented grains.

The lattice parameters (a and c) of the synthesized ZnO thin films were calculated using Equation (2), while the interplanar spacing (d) was determined from Bragg's law, Equation (3) [24]:

$$a = \frac{\lambda}{\sqrt{3}\sin(\theta)} \text{ and } c = \frac{\lambda}{\sin(\theta)} \quad (2)$$

$$d = \frac{\lambda}{2sin\theta} \quad (3)$$

Where θ is the Bragg angle, λ is the wavelength of the incident X-rays (λ = 1.506 Å).

The crystallite size (D) of the ZnO thin films was estimated from the XRD diffraction peaks using the Scherrer Equation (4) [16]:

$$D = \frac{k\lambda}{\beta \cos\theta} \quad (4)$$

where β is the full width at half maximum (FWHM), k is a shape constant approximately equal to 0.9, and θ is the Bragg diffraction angle.

The dislocation density (δ), which reflects the density of crystalline defects in the films, was estimated using Equation (5) [25]:

$$\delta = \frac{1}{D^2} \quad (5)$$

The strain ε used to verify the stress in ZnO thin films was calculated using Equation (6) [23]:

$$\varepsilon = \frac{\beta}{4\tan\theta} \quad (6)$$

where β is the width at half-height and θ is the diffraction angle.

The volume of the hexagonal cell (V) was calculated using Equation (7) [13]:

$$V = \frac{\sqrt{3}}{2}a^2c \quad (7)$$

The bond length (L) of Zn-O was calculated using Equation (8) [13]:

$$L = \sqrt{\left[\frac{a^2}{3} + \left(\frac{1}{2} - u\right)^2 c^2\right]}, \text{ with } u = \frac{a^2}{3c^2} + \frac{1}{4} \quad (8)$$

where u is the positional parameter of the wurtzite structure, representing the displacement of atoms along the c-axis relative to the basal plane.

3. Results and Discussion

3.1. Structural Characterization

Figure 3 presents the X-ray diffraction (XRD) patterns of

ZnO thin films synthesized at different growth times. The results indicate that growth time has a significant influence on the crystallographic orientation and structural quality of the films. The diffraction peaks are indexed using the standard hexagonal wurtzite ZnO structure (JCPDS card No. 36-1451), confirming the formation of ZnO with space group $P6_3mc$ [26]. All the films exhibit a polycrystalline nature, with diffraction peaks observed at approximately $2\theta \approx 31.7°$, 34.4°, and 36.2°, corresponding to the (100), (002), and (101) crystallographic planes of ZnO, respectively. No additional diffraction peaks related to secondary crystalline phases, such as $Zn(OH)_2$, are detected within the resolution limit of the XRD measurements. However, the possible presence of minor amorphous or nanocrystalline impurity phases below the detection threshold cannot be completely excluded.

A clear evolution in crystallinity is observed with increasing growth time. In particular, the intensity of the (002) diffraction peak increases markedly with growth duration, indicating an enhancement in crystallinity and a progressive preferential orientation along the c-axis. In contrast, the almost complete absence of diffraction peaks for the sample grown for 1 hour suggests incomplete crystallization and insufficient structural development at short growth times. Overall, the XRD results confirm that extended growth time promotes improved structural ordering and enhances the crystalline quality of the ZnO films.

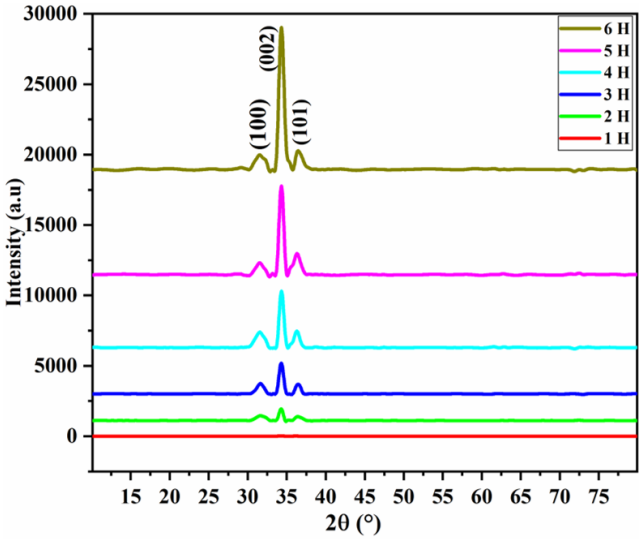

Figure 3. *XRD patterns of ZnO thin films synthesized at different growth times.*

The diffraction angles corresponding to the dominant peaks are summarized in Table 1 for the different growth times. Slight variations in the 2θ positions are observed with increasing growth time. These shifts may be attributed to variations in internal stress and crystalline quality resulting from the interaction between the ZnO films and the glass substrates [24, 27, 28].

Table 1. *Variation of the diffraction angles 2θ of the dominant peaks for each growth time.*

(hkl)	Growth time						JCPDS card 36-1451
	1 h	2 h	3 h	4 h	5 h	6 h	
(100)	31.645	31.677	31.617	31.546	31.539	31.574	31.770
(002)	34.238	34.268	34.297	34.331	34.331	34.325	34.422
(101)	36.108	36.518	36.458	36.282	36.303	36.588	36.253

The texture coefficients calculated using Equation (1) are presented in Table 2. The obtained results show that the $T_{C(100)}$ and $T_{C(101)}$ values remain lower than unity, indicating weaker growth along these crystallographic directions compared with the standard JCPDS data [29]. In contrast, the $T_{C(002)}$ values are greater than 1 for all samples, confirming the preferential orientation of the films along the c-axis. This preferred orientation is associated with the anisotropic growth behavior of ZnO crystallites during the hydrothermal process [30]. The sharp and intense diffraction peaks further indicate the high crystalline quality of the deposited films, in good agreement with previous reports [31, 32].

Table 2. *Texture coefficients of ZnO thin films synthesized at different growth times for the dominant crystallographic planes (100), (002), and (101).*

Growth time	$T_{C(hkl)}$		
	(100)	(002)	(101)
1 h	0.4	2.0	0.5
2 h	0.7	2.1	0.3
3 h	0.6	2.2	0.3

Growth time	$T_{C(hkl)}$		
	(100)	(002)	(101)
4 h	0.5	2.3	0.3
5 h	0.3	2.4	0.3
6 h	0.3	2.6	0.2

The lattice parameters calculated using Equation (2) are listed in Table 3. The obtained values are close to those reported the standard JCPDS card No. 36-1451 [26], confirming the formation of high-quality hexagonal ZnO films. A slight increase in the lattice parameters is observed with increasing growth time, which may be related to residual stress and lattice distortion induced by the mismatch between the ZnO films and the glass substrates [33]. Moreover, the c/a ratio remains nearly constant at approximately 1.6 for all samples, indicating that the films preserve the characteristic hexagonal wurtzite structure throughout the growth process.

The interplanar spacing (d) values, calculated using Bragg's law, Equation (3), for the dominant (100), (002), and (101) planes, are also presented in Table 3. Only slight variations are observed with increasing growth time, and the obtained values remain close to the standard JCPDS data. This consistency confirms the structural stability of the ZnO thin films during hydrothermal growth.

The full width at half maximum (FWHM) values extracted from the dominant diffraction peaks decrease progressively from 0.742° to 0.566° with increasing growth time, as shown in Table 3. The reduction in FWHM indicates an improvement in crystallinity accompanied by an increase in crystallite size for longer growth durations. This behavior reflects the progressive coalescence and improved organization of ZnO crystallites during hydrothermal growth [34].

The crystallite size and dislocation density of the ZnO thin films are estimated from the dominant (002) diffraction peak using the Scherrer relation, Equation (4) and Equation (5), respectively. The results summarized in Table 3 show that the crystallite size increases from 11.19 to 14.67 nm as the growth time increases, indicating enhanced crystal growth during prolonged hydrothermal deposition. This increase may be associated with the gradual coalescence of crystallites and grain growth processes, consistent with previous studies reported by Siregar et al. [35] et Gboglo et al. [13]. Simultaneously, the dislocation density decreases with increasing growth time, suggesting a reduction in crystal imperfections and an improvement in crystalline quality.

Table 3. *Structural parameters of ZnO thin films determined from the (002) diffraction peak at different growth times.*

Growth time	Lattice parameters			$d_{(002)}$ (Å)	β (°)	D (nm)	δ (10^{14} lines/m^2)	ε ($\times 10^{-3}$)	V (Å^3)	L (Å)
	a (Å)	c (Å)	c/a							
1 h	3.262	5.234	1.604	2.616	0.742	11.192	79.831	10.496	48.328	1.987
2 h	3.260	5.229	1.605	2.614	0.736	11.290	78.443	10.421	48.235	1.986
3 h	3.265	5.225	1.600	2.612	0.643	12.911	59.987	9.105	48.237	1.986
4 h	3.272	5.220	1.595	2.610	0.649	12.795	61.074	9.179	48.403	1.988
5 h	3.273	5.223	1.596	2.611	0.649	12.808	60.958	9.175	48.450	1.989
6 h	3.261	5.221	1.597	2.610	0.566	14.672	46.448	8.019	48.100	1.984
JCPDS card 36-1451	3.250	5.207	1.602	2.603		-	-	-	47.622	-

The strain values calculated using Equation (6) and presented in Table 3 decrease progressively with increasing growth time. The positive strain values indicate tensile lattice deformation [12, 36], which may originate from thermal mismatch between the ZnO films and the glass substrates during the annealing process [13]. The reduction in strain with prolonged growth time suggests a gradual relaxation of internal stresses and improved structural ordering within the films.

The lattice volume V, calculated using Equation (7), exhibits slight fluctuations with growth time. These variations are mainly associated with small shifts in diffraction peak positions, which directly influence the calculated lattice parameters. In addition, the Zn–O bond length (L), determined using Equation (8), shows only minor variations, confirming the structural stability of the synthesized ZnO films [11]. The relative stability of the Zn–O bond length indicates that the local atomic arrangement within the wurtzite lattice remains largely preserved throughout the growth process [12].

3.2. Optical Characterization

3.2.1. UV–Visible Spectroscopy

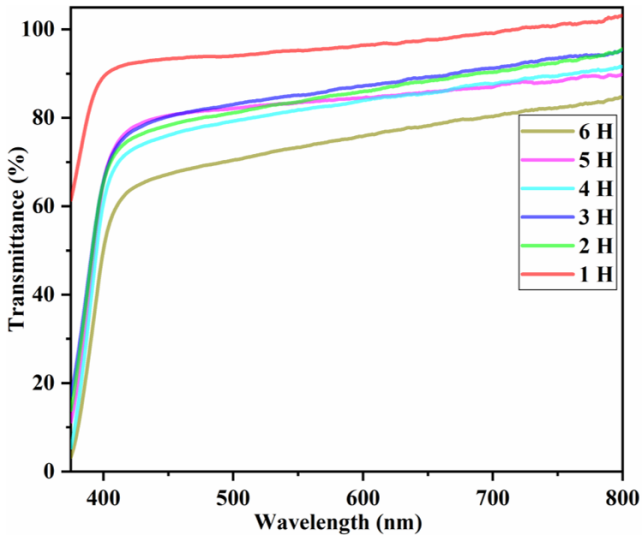

Figure 4. *Transmission spectra of thin ZnO films synthesized at different growth times.*

Figure 4 shows the UV–visible transmittance spectra of ZnO thin films synthesized at different growth times. The results reveal a continuous decrease in optical transmittance with increasing growth time, from approximately 95% to 65%. Although film thickness and surface morphology were not experimentally evaluated, the observed variations in the optical response with growth time may be associated with changes in film thickness, densification, and structural uniformity, which enhance light–matter interactions and scattering within the films [37, 38].

A sharp absorption edge is observed in the ultraviolet region below ~388 nm, corresponding to the intrinsic band-to-band transition of ZnO (valence band to conduction band) [27].

A systematic red shift of the absorption edge is observed with increasing growth time. This effect is particularly evident for the film grown for 1 h, which exhibits a noticeable absorption tail extending into the visible region. Such behavior is generally associated with incomplete crystallization and a higher density of structural disorder. This absorption tail can be attributed to defect-related localized states, increased surface roughness, and/or sub-bandgap states within the forbidden energy gap. This interpretation is consistent with the XRD results, which indicate lower crystallinity and broader diffraction peaks for the same sample.

An optimal growth window is identified between 2 and 4 h, where the films exhibit a favorable optical balance characterized by high transparency in the visible region and strong absorption in the ultraviolet range. This combination is particularly desirable for photoanode applications, where efficient UV harvesting and high visible transparency are required.

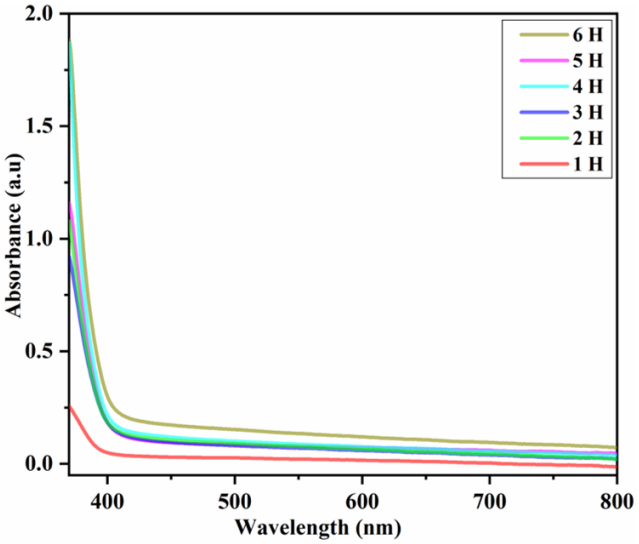

Figure 5. *Absorption spectra of ZnO thin films synthesized at different growth times.*

Figure 5 presents the corresponding absorption spectra as a function of wavelength. Strong absorption is observed in the UV region ($\lambda < 380$ nm), confirming the capability of ZnO films to efficiently absorb high-energy photons and generate electron–hole pairs through optical excitation. In contrast, low absorption in the visible and near-infrared regions ($\lambda > 380$ nm) confirms their high transparency, which is consistent with the transmittance results.

3.2.2. Photoluminescence (PL) Spectroscopy

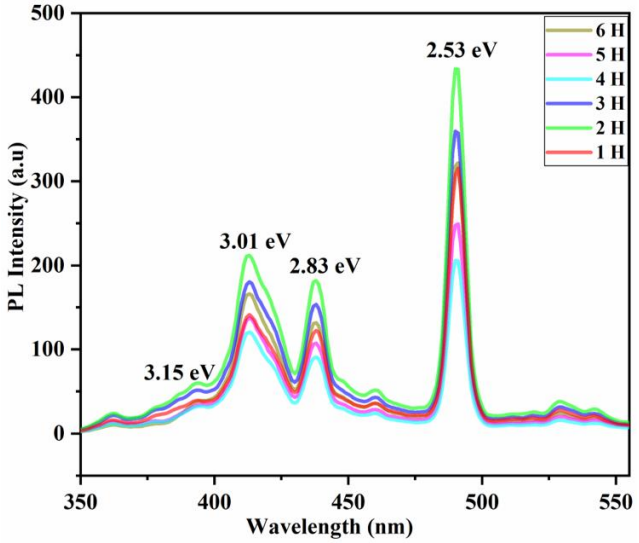

Figure 6. *Photoluminescence spectra of ZnO thin films synthesized at different growth times.*

Figure 6 presents the photoluminescence (PL) spectra of ZnO thin films grown for different durations. The PL spectra exhibit two main emission regions. The first corresponds to a

narrow ultraviolet (UV) emission centered around ~380 nm (3.15 eV), attributed to near-band-edge (NBE) excitonic recombination. The presence of this emission is generally associated with good crystalline quality due to the wide direct bandgap (~3.37 eV) and high exciton binding energy (~60 meV) of ZnO [39].

The second contribution is a broad visible emission band, commonly associated with intrinsic defects within the ZnO lattice, including oxygen vacancies, zinc interstitials, and defect complexes [40]. All investigated samples exhibit emission bands in both the UV and visible regions, with dominant visible emissions located in the blue region at approximately 412 nm (3.01 eV), 438 nm (2.83 eV), and 490 nm (2.53 eV). The variation in PL intensity with growth time indicates that the deposition duration strongly influences defect formation and the optical properties of the ZnO thin films. According to previous reports, the intensity of the UV emission is closely related to the crystallinity of ZnO films. All photoluminescence measurements were carried out under identical experimental conditions; thus, the weak near-band-edge emission relative to the visible defect-related emission is mainly attributed to intrinsic structural defects within the ZnO thin films rather than experimental parameters.

According to the literature, UV emission is commonly considered an indicator of improved crystallinity [40]. However, the relatively weak UV emission compared to the visible emission suggests a significant density of intrinsic defects in the films. These defect-related emissions are generally attributed to radiative transitions involving the conduction band and defect states such as oxygen vacancies and zinc-related defects [40–42]. Among the investigated samples, the film grown for 2 h exhibits the highest visible emission intensity, indicating a higher concentration of structural defects. In contrast, the film synthesized for 4 h shows the lowest visible emission intensity, suggesting reduced defect density and improved crystalline quality [43]. These observations are consistent with the XRD results, which revealed enhanced crystallinity and reduced structural disorder with increasing growth time.

3.2.3. Optical Bandgap Energy of ZnO Thin Films Synthesized

The optical bandgap energy of the ZnO thin films was determined using the derivative method based on the transmittance spectra. The derivative of transmittance (dT/dλ) was plotted as a function of photon energy (hν), as shown in Figure 7, allowing accurate estimation of the bandgap values [44]. The extracted bandgap values, summarized in Table 4, range from 3.14 eV to 3.27 eV depending on growth time. This variation is attributed to changes in crystallite size, structural disorder, and defect density, consistent with the XRD and PL results. Overall, the obtained bandgap values are slightly lower than that of bulk ZnO (3.37 eV), which may be attributed to the presence of residual strain, structural defects, and quantum confinement effects associated with the nanoscale nature of the films [45, 46].

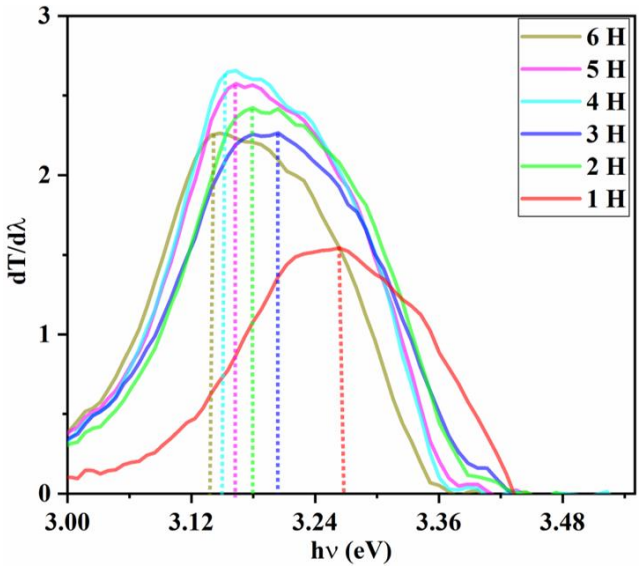

Figure 7. dT/dλ curve as a function of photon energy for ZnO thin films prepared at different growth times.

Table 4. Band gap values of ZnO thin films grown for different durations.

Growth time	Band gap energy (eV)
1 h	3.27
2 h	3.18
3 h	3.20
4 h	3.15
5 h	3.16
6 h	3.14

4. Conclusions

In this work, the influence of growth time on the structural and optical properties of hydrothermally synthesized ZnO thin films was systematically investigated. XRD analysis revealed that all deposited films crystallize in the hexagonal wurtzite structure with a preferential orientation along the (002) plane, indicating dominant c-axis growth. The progressive increase in the intensity of the (002) diffraction peak with growth time confirms a significant improvement in crystalline quality and structural ordering. UV–visible spectroscopy showed that the ZnO thin films maintain high optical transparency in the visible region while exhibiting strong ultraviolet absorption. A decrease in transmittance with increasing growth time was observed, mainly due to enhanced film densification and thickness. Films grown for 2–4 h exhibited the most favorable op-

tical behavior, combining high visible transparency with efficient UV absorption, which is desirable for photovoltaic applications. Photoluminescence measurements revealed defect-related visible emissions centered in the blue region. The reduction in visible emission intensity for the film grown for 4 h indicates a lower density of intrinsic defects and improved crystalline quality. These observations are in good agreement with the XRD results, confirming the strong correlation between growth time, crystallinity, and defect formation. Overall, the results demonstrate that growth time is a key parameter governing the structural and optical properties of hydrothermally synthesized ZnO thin films. Among the investigated samples, the film grown for 4 h exhibits the most promising combination of high crystallinity, reduced defect density, and good optical transparency, making it a suitable candidate for photoanode applications in photovoltaic devices. From a broader perspective, this study highlights the importance of optimizing growth kinetics to tailor the balance between crystallinity, defect density, and optical performance in ZnO-based nanostructures. Future work should include direct measurements of film thickness and surface morphology (e.g., profilometry and SEM/AFM analyses) to provide a more complete understanding of the relationship between growth conditions and microstructural evolution. In addition, extending this approach to full photovoltaic device fabrication and performance evaluation would further validate the applicability of the optimized ZnO thin films in practical energy conversion systems.

Abbreviations

ZnO	Zinc Oxide
TiO_2	Titanium Dioxide
HMTA	Hexamethylenetetramine
FWHM	Full Width at Half Maximum
XRD	X-ray Diffraction
UV	Ultraviolet
UV-Vis	Ultraviolet-visible Spectroscopy
PL	Photoluminescence
NBE	Near-Band-Edge
SEM	Scanning Electron Microscopy
AFM	Atomic Force Microscopy
JCPDS	Joint Committee on Powder Diffraction Standards
CERME	Centre d'Excellence Régional Pour la Maîtrise de l'Electricité

Acknowledgments

The authors gratefully acknowledge CERME (Togo) for financial support. The authors also thank Alagappa Govt. Arts College (India) for providing technical support for formal analysis.

Author Contributions

Mazabalo Baneto: Conceptualization, Methodology, Supervision, Writing – review & editing

Jeanne Senam Aklamanu: Conceptualization, Data curation, Methodology, Writing – original draft

Alphonse Déssoudji Gboglo: Data curation, Methodology, Writing – original draft, Writing – review & editing

Ognanmi Ako: Data curation, Formal Analysis, Writing – review & editing

Abdoul-Razak Ali-Tagba: Data curation, Formal Analysis, Visualization

Monneka Fiacre Kouide: Formal Analysis, Resources, Visualization

Danoka Djagbai: Investigation, Resources, Visualization

Makadatièna Badjemna: Investigation, Visualization, Resources

Akotchayé Amenou: Formal Analysis, Visualization, Resources

Funding

This work is not supported by any external funding.

Data Availability Statement

The original contributions presented in this study are included in the article. Further inquiries can be directed to the corresponding author.

Conflicts of Interest

The authors declare no conflicts of interest.

References

[1] A. Ejsmont, J. Goscianska, Hydrothermal Synthesis of ZnO Superstructures with Controlled Morphology via Temperature and pH Optimization, Materials 16 (2023) 1641. https://doi.org/10.3390/ma16041641

[2] P. Dhanasekaran, R. Marimuthu, A Review on Dye-Sensitized Solar Cells (DSSCs), Materials and Applications, Iran. J. Mater. Sci. Eng. 20 (2023). https://doi.org/10.22068/ijmse.2994

[3] A. Taleb, F. Mesguich, A. Hérissan, C. Colbeau-Justin, X. Yanpeng, P. Dubot, Optimized TiO_2 nanoparticle packing for DSSC photovoltaic applications, Sol. Energy Mater. Sol. Cells 148 (2016) 52–59. https://doi.org/10.1016/j.solmat.2015.09.010

[4] M. Z. Hossain, S. M. A. Nayem, S. Alam, I. Islam, G. Seong, A.-N. Chowdhury, Hydrothermal ZnO Nanomaterials: Tailored Properties and Infinite Possibilities, Nanomaterials 15 (2025) 609. https://doi.org/doi.org/10.3390/nano15080609

[5] A. D. Gboglo, M. Baneto, O. Ako, A.-R. Ali-Tagba, B. Grandidier, K. N'konou, Combined Influence of Precursor Source and Solvent Type on Microstructural and Optical Properties of Spin-Coated ZnO Thin Films, Surfaces 9 (2026) 50. https://doi.org/10.3390/surfaces9020050

[6] N. Zhang, K. Yu, L. Li, Z. Zhu, Investigation of electrical and ammonia sensing characteristics of Schottky barrier diode based on a single ultra-long ZnO nanorod, Appl. Surf. Sci. 254(2008): 5736–5740. https://doi.org/10.1016/j.apsusc.2008.03.039

[7] F. T. Z. Toma, M. S. Rahman, K. H. Maria, A review of recent advances in ZnO nanostructured thin films by various deposition techniques, Discov. Mater. 5 (2025) 60. https://doi.org/doi.org/10.1007/s43939-025-00201-1

[8] P. Sigmund, Theory of Sputtering. I. Sputtering Yield of Amorphous and Polycrystalline Targets, Phys. Rev. 184 (1969) 383–416. https://doi.org/10.1103/PhysRev.184.383

[9] J. L. H. Chau, M.-C. Yang, T. Nakamura, S. Sato, C.-C. Yang, C.-W. Cheng, Fabrication of ZnO thin films by femtosecond pulsed laser deposition, Opt. Laser Technol. 42 (2010) 1337–1339. https://doi.org/10.1016/j.optlastec.2010.04.015

[10] S. FaÿU. Kroll, C. Bucher, E. Vallat -Sauvain, A. Shah, Low pressure chemical vapour deposition of ZnO layers for thin-film solar cells: temperature-induced morphological changes, Sol. Energy Mater. Sol. Cells 86 (2005) 385–397. https://doi.org/10.1016/j.solmat.2004.08.002

[11] E. Heredia, C. Bojorge, J. Casanova, H. Cánepa, A. Craievich, G. Kellermann, Nanostructured ZnO thin films prepared by sol–gel spin-coating, Appl. Surf. Sci. 317 (2014) 19–25. https://doi.org/10.1016/j.apsusc.2014.08.046

[12] O. Ako, M. Baneto, A. D. Gboglo, M. Senthilkumar, M. Haris, Temperature-controlled growth of ZnO Thin films by spray pyrolysis: Influence on physical properties for photovoltaic applications, Edelweiss Appl. Sci. Technol. 9 (2025) 1052–1066. https://doi.org/10.55214/2576-8484.v9i10.10594

[13] A. D. Gboglo, M. Baneto, O. Ako, K. S. Gadedjisso-Tossou, B. Grandidier, M. Haris, M. Senthilkumar, K. N'Konou, Structural, morphological and optical properties of ZnO thin films grown by time-dependent chemical bath deposition, Int. J. Renew. Energy Dev. 15 (2026) 66–75. https://doi.org/10.61435/ijred.2026.61665

[14] D. Polsongkram, P. Chamninok, S. Pukird, L. Chow, O. Lupan, G. Chai, H. Khallaf, S. Park, A. Schulte, Effect of synthesis conditions on the growth of ZnO nanorods via hydrothermal method, Phys. B Condens. Matter 403 (2008) 3713–3717. https://doi.org/10.1016/j.physb.2008.06.020

[15] H. S. Wasly, M. S. A. El-Sadek, M. Henini, Influence of Reaction Time and Synthesis Temperature on Physical Properties of ZnO Nanoparticles Synthesized by Hydrothermal Method, Appl. Phys. A 124 (2018). https://doi.org/doi.org/10.1007/s00339-017-1482-4

[16] M. M. Kareem, Z. T. Khodair, F. Y. Mohammed, Effect of annealing temperature on structural, morphological and optical properties of zno nanorod thin films prepared by hydrothermal method, J. Ovonic Res. 16 (2020) 53–61. https://doi.org/10.15251/JOR.2020.161.53

[17] Y. T. Yin, W. X. Que, C. H. Kam, ZnO nanorods on ZnO seed layer derived by sol–gel process, J. Sol-Gel Sci. Technol. 53 (2010) 605–612. https://doi.org/10.1007/s10971-009-2138-4

[18] A. Dloo, N. Fazouan, E. H. Atmani, Investigation of hydrothermal growth time and temperature for optimized ZnO nanowire arrays toward photovoltaics, Surf. Interfaces 40 (2023) 103123. https://doi.org/10.1016/j.surfin.2023.103123

[19] G. Amin, M. H. Asif, A. Zainelabdin, S. Zaman, O. Nur, M. Willander, Influence of pH, Precursor Concentration, Growth Time, and Temperature on the Morphology of ZnO Nanostructures Grown by the Hydrothermal Method, J. Nanomater. 2011 (2011) 1–9. https://doi.org/10.1155/2011/269692

[20] E. M. Abdel-Fattah, S. M. Alshehri, Effect of Hydrothermal Reaction Time on the Morphological and Photocatalytic Properties of ZnO Nanostructures, Appl. Sci. 16 (2026) 1408. https://doi.org/10.3390/app16031408

[21] S. Abou Zeid, A. Perez, S. Bastide, S. Rossano, Y. Leprince-Wang, Time-Dependent Growth of ZnO Nanowires: Unveiling Antibacterial and Photocatalytic Properties, Langmuir 41 (2025) 2237–2247. https://doi.org/10.1021/acs.langmuir.4c03709

[22] H. Ebrahimi, H. Yaghoubi, F. Giammattei, A. Takshi, Electrochemical Detection of Piezoelectric Effect from Misaligned Zinc Oxide Nanowires Grown on a Flexible Electrode, Electrochimica Acta 134 (2014) 435–441. https://doi.org/10.1016/j.electacta.2014.04.119

[23] R. Rai, T. Triloki, B. K. Singh, X-ray diffraction line profile analysis of KBr thin films, Appl. Phys. A 122 (2016) 774. https://doi.org/10.1007/s00339-016-0293-3

[24] M. Baneto, D. Djagbai, E. Mouzou, A. D. Gboglo, O. Ako, M. F. Kouide, D. Kassegne, Controlled Deposition of Zn Thin Films by Spin Coating: Influence of Spin Speed on Film Microstructure and Transparency, J. Nano- Electron. Phys. 17 (2025) 05016-1-05016–8. https://doi.org/10.21272/jnep.17(5).05016

[25] G. K. Williamson, R. E. Smallman, III. Dislocation densities in some annealed and cold-worked metals from measurements on the X-ray debye-scherrer spectrum, Philos. Mag. 1 (1956) 34–46. https://doi.org/10.1080/14786435608238074

[26] H. F. McMurdie, M. C. Morris, E. H. Evans, B. Paretzkin, W. Wong-Ng, L. Ettlinger, C. R. Hubbard, Standard X-Ray Diffraction Powder Patterns from the JCPDS Research Associateship, Powder Diffr. 1 (1986) 64–77. https://doi.org/10.1017/S0885715600011593

[27] A. D. Gboglo, M. Baneto, O. Ako, M. Haris, M. Senthilkuma, Role of hexamethylenetetramine/zinc nitrate hexahydrate molar ratio in controlling structural, morphological and optical properties of ZnO thin films synthesized by CBD, AIMS Mater. Sci. 12 (2025) 893–908. https://doi.org/10.3934/matersci.2025039

[28] O. Ako, M. Baneto, M. Senthilkumar, M. Haris, A. D. Gboglo, K. S. Gadedjisso-Tossou, A. C. Ahyi, K. Beltako, K. A. Amou, Simultaneous effect of precursor sources and concentration on structural, morphological and optical properties of ZnO nanostructured thin films for photovoltaic applications, Int. J. Renew. Energy Dev. 14 (2025) 495–504. https://doi.org/10.61435/ijred.2025.61069

[29] P. Obreja, D. Cristea, A. Dinescu, C. Romaniţan, Influence of surface substrates on the properties of ZnO nanowires synthesized by hydrothermal method, Appl. Surf. Sci. 463 (2019) 1117–1123. https://doi.org/10.1016/j.apsusc.2018.08.191

[30] A. M. Alsaad, A. A. Ahmad, Q. M. Al-Bataineh, A. A. Bani-Salameh, H. S. Abdullah, I. A. Qattan, Z. M. Albataineh, A. D. Telfah, Optical, Structural, and Crystal Defects Characterizations of Dip Synthesized (Fe-Ni) Co-Doped ZnO Thin Films, Materials 13 (2020) 1737. https://doi.org/10.3390/ma13071737

[31] M. Arellano-Cortaza, E. Ramírez-Morales, U. Pal, G. Pérez-Hernández, L. Rojas-Blanco, pH dependent morphology and texture evolution of ZnO nanoparticles fabricated by microwave-assisted chemical synthesis and their photocatalytic dye degradation activities, Ceram. Int. 47(2021): 27469–27478. https://doi.org/10.1016/j.ceramint.2021.06.170

[32] M. N. Kamalasanan, S. Chandra, Sol-gel synthesis of ZnO thin films, Thin Solid Films 288(1996): 112–115. https://doi.org/10.1016/S0040-6090(96)08864-5

[33] A. F. Abdulrahman, S. M. Ahmed, N. M. Ahmed, M. A. Almessiere, Enhancement of ZnO Nanorods Properties Using Modified Chemical Bath Deposition Method: Effect of Precursor Concentration, Crystals 10 (2020) 386. https://doi.org/10.3390/cryst10050386

[34] L. M. Balcazar, M. D. L. L. Olvera Amador, IGZO thin films deposited by ultrasonic spray pyrolysis: effect of Zn precursor milling and In and Ga concentration, J. Mater. Sci. Mater. Electron. 35 (2024) 829. https://doi.org/10.1007/s10854-024-12412-y

[35] N. Siregar, M. Motlan, M. Sirait, Electroplated ZnO Thin Film: Influence of Deposition Time on Optical and Structural Properties, J. Phys. Sci. 34 (2023) 43–55. https://doi.org/10.21315/jps2023.34.1.4

[36] A. D. Gboglo, M. Baneto, K. S. Gadedjisso-Tossou, O. Ako, A. C. Ahyi, M. Haris, M. Senthilkumar, K. N'konou, B. Grandidier, K. Beltako, K. A. Amou, M. M. Dzagli, Co-Effect of pH Control Agent and pH Value on the Physical Properties of ZnO Thin Films Obtained by Chemical Bath Deposition for Potential Application in Dye-Sensitized Solar Cells, Surfaces 8 (2025) 46. https://doi.org/10.3390/surfaces8030046

[37] V. Khranovskyy, T. Ekblad, R. Yakimova, L. Hultman, Surface morphology effects on the light-controlled wettability of ZnO nanostructures, Appl. Surf. Sci. 258 (2012) 8146–8152. https://doi.org/10.1016/j.apsusc.2012.05.011

[38] D. Sengupta, P. Das, U. Kasinadhuni, B. Mondal, K. Mukherjee, Morphology induced light scattering by zinc oxide polydisperse particles: Promising for dye sensitized solar cell application, J. Renew. Sustain. Energy 6 (2014) 063114. https://doi.org/10.1063/1.4904435

[39] E. Musavi, M. Khanlary, Z. Khakpour, Red-orange photoluminescence emission of sol-gel dip-coated prepared ZnO and ZnO: Al nano-crystalline films, J. Lumin. (2019). https://doi.org/10.1016/j.jlumin.2019.116696

[40] Y. Li, L. Xu, X. Li, X. Shen, A. Wang, Effect of aging time of ZnO sol on the structural and optical properties of ZnO thin films prepared by sol–gel method, Appl. Surf. Sci. 256 (2010) 4543–4547. https://doi.org/10.1016/j.apsusc.2010.02.044

[41] A. Galdámez-Martinez, G. Santana, F. Güell, P. R. Martínez-Alanis, A. Dutt, Photoluminescence of ZnO Nanowires: A Review, Nanomaterials 10 (2020) 857. https://doi.org/10.3390/nano10050857

[42] J. Li, D. Yang, X. Zhu, Effects of aging time and annealing temperature on structural and optical properties of sol-gel ZnO thin films, AIP Adv. 7 (2017) 065213. https://doi.org/10.1063/1.4985753

[43] E. A. Araújo Júnior, F. X. Nobre, G. D. S. Sousa, L. S. Cavalcante, M. Rita De Morais Chaves Santos, F. L. Souza, J. M. Elias De Matos, Synthesis, growth mechanism, optical properties and catalytic activity of ZnO microcrystals obtained via hydrothermal processing, RSC Adv. 7(2017): 24263–24281. https://doi.org/10.1039/C7RA03277C

[44] L. Xu, X. Wang, L. Qian, Y. Zhu, X. Luo, W. Wang, X. Xu, J. Xu, The dependence of the optical properties of ZnO nanorod arrays on their growth time, Optik 202 (2020) 163634. https://doi.org/10.1016/j.ijleo.2019.163634

[45] R. Marotti, Bandgap energy tuning of electrochemically grown ZnO thin films by thickness and electrodeposition potential, Sol. Energy Mater. Sol. Cells 82 (2004) 85–103. https://doi.org/10.1016/j.solmat.2004.01.008

[46] K. L. Foo, U. Hashim, K. Muhammad, C. H. Voon, Sol–gel synthesized zinc oxide nanorods and their structural and optical investigation for optoelectronic application, Nanoscale Res. Lett. 9(2014): 429. https://doi.org/10.1186/1556-276X-9-429